View metadata, citation and similar papers at core.ac.uk
brought to you by CORE
provided by NASA Technical Reports Server

N78-24073

ACOUSTIC-LOADS RESEARCH FOR POWERED-LIFT CONFIGURATIONS

James A. Schoenster, Conrad M. Willis,
James C. Schroeder, and John S. Mixson,
NASA Langley Research Center

SUMMARY

Intense noise sources are associated with the impingement of the jet engine exhaust on the wing and flap surfaces of powered-lift configurations. These noise sources may cause excessive noise inside the aircraft or may induce early acoustic fatigue failure. A current research program is aimed at determining the acoustic loads on the aircraft surfaces due to the impingement noise for use in studies of acoustic fatigue and interior noise control and at developing methods for predicting the loads. The research program includes acoustic-loads measurements on a variety of configurations including small-scale models, large-scale models, and flight vehicles. Companion analytical studies seek to develop and verify scaling laws for prediction of flight values from scale-model tests. Data presented from large-scale model tests with jet engines having thrusts of 9 kN (2000 lb) and 36 kN (8000 lb) include acoustic loads for an externally blown wing and flap induced by a TF34 jet engine, an upper surface blown (USB) aircraft model in a wind tunnel, and two USB models in static tests. Comparisons of these results with results from acoustic-loads studies on configurations of other sizes are made and the implications of these results on interior noise and acoustic fatigue are discussed.

INTRODUCTION

Two of the powered-lift configurations receiving considerable attention for use in short take-off and landing (STOL) aircraft are the externally blown flap (EBF) system and the upper-surface blown (USB) system. To obtain the additional lift, both these configurations require the jet engine exhaust to impinge directly on the wing-flap structures of the aircraft. The effects of this impingement are (1) to increase the overall fluctuating loads on the aircraft above the level normally encountered by conventional aircraft and (2) to concentrate the peak levels of these fluctuating loads at lower frequencies than normally encountered. The results of these high levels and the low-frequency content are (1) to increase the potential of sonic fatigue and (2) to induce high acoustic levels in the interior of the aircraft. The extent of these problems in powered-lift aircraft is shown in figures 1 and 2. Figure 1, taken from reference 1, shows that sonic fatigue failures of small secondary structures have occurred for a wide variety of sources when levels exceed 130 dB. Above this level, special design considerations are needed to minimize the potential of failure. Figure 2, taken from reference 2, illustrates the potential interior noise problems of STOL aircraft. Figure 2(a) shows the external noise

spectrum for a USB take-off configuration. Figure 2(b) indicates the current technology of aircraft sidewall noise reduction. Figure 2(c) shows the resulting USB interior noise spectrum based on the data in figures 2(a) and (b). Also shown, for reference purposes, in figure 2(c) are spectral data measured during cruise conditions on CTOL aircraft. These predictions indicate that in the lower frequency range, interior noise levels are 25 dB above those for current cruise aircraft - a considerably noisier interior environment.

Because of these potential problem areas, a program designed to develop techniques for predicting fluctuating loads on STOL aircraft was established at Langley Research Center. The effects of these predicted loads could then be incorporated in the design of the aircraft to prevent many problems that otherwise would require modifications after the aircraft was built. It was believed that the use of models would be the best approach. Shown in figure 3 is an outline of the program which developed. To aid in determining scaling laws and prediction methods, three types of models were selected for investigation: small-scale models, large-scale models, and flight vehicles. Langley has directly supported or conducted in-house tests on all three types of models for both the EBF configuration and the USB configuration.

SYMBOLS

d	jet nozzle exit diameter, m
f	frequency, Hz
M_j	Mach number of the jet at the nozzle exit
p_{rms}	root-mean-square value of the fluctuating pressure, Pa
q_o	dynamic pressure of the jet at the nozzle exit, Pa
U_0	velocity of the jet at the nozzle exit, m/sec

ABBREVIATIONS

AMST	advanced medium short take-off and landing transport
BBN	Bolt Beranek and Newman
EBF	externally blown flap
FPL	fluctuating pressure level
OA	overall
OAFPL	overall fluctuating pressure level

PSD power spectral density

SPL sound pressure level

USB upper-surface blown

EBF FLUCTUATING-LOADS STUDIES

Shown in figure 4 are photographs of the test configurations being used to study the EBF fluctuating loads. At the lower left is the Bolt Beranek and Newman (BBN) EBF small-scale model. Data from this model have been reported in reference 3. In the middle photograph is the TF34 engine (36 kN (8000 lb) thrust) EBF model which was tested at the NASA Lewis Research Center. Preliminary data from this test have been reported in references 4 and 5. Shown at the top of the figure is the Douglas AMST YC-15 aircraft. The YC-15 is currently undergoing flight evaluation tests by the U.S. Air Force, and in the spring of 1976, fluctuating-loads data were obtained on the wing, flap, and fuselage. In addition, Langley Research Center in cooperation with the Air Force Flight Dynamics Laboratory has obtained data on the structural response of the fuselage sidewall and on interior noise levels of this aircraft. These data are not currently available for publication.

Overall fluctuating pressure levels (OAFPL), in decibels referenced to 20μPa, measured on the TF34 EBF model are shown in table I. Shown in schematic view are the engine, the wing, and the flap settings for typical take-off (flap angles of 0°, 20°, and 40°) and landing (flap angles of 15°, 35°, and 55°) configurations. Listed in the table are measurements obtained at flap locations on a vertical plane through the engine center line. The measurements cover a range of jet exhaust Mach numbers from 0.33 to 0.59. The highest levels were 163 dB for the take-off flap setting and 162 dB for the landing flap setting. However, in all cases, the table shows levels equal to or exceeding 143 dB, clearly above the level indicated in figure 1 for the onset of acoustic fatigue problems.

Although the BBN small-scale model is not an exact replica of the TF34 model, it is approximately a 1/20-scale model. Nondimensionalized data from both models obtained at transducer locations 2 and 5 (see sketch in table I) for both a take-off configuration and a landing configuration are shown in figure 5. The frequency scale is nondimensionalized by using the nozzle exit diameter and nozzle exit jet velocity as parameters. This normalized value is called the Strouhal number. The mean-square fluctuating pressure levels in 1/3-octave bandwidths and normalized to the jet dynamic pressure at the exit are plotted in decibels on the vertical scale. Data from the models collapse very well for both flaps in the take-off configuration and for the aft flap in the landing configuration (figs. 5(a), (b), and (d)). Normalized amplitudes are well within 5 dB of each other and the peak response generally occurs at a Strouhal number between 0.4 and 0.5. The peak response is at a somewhat lower Strouhal number (0.27) on the aft flap in the take-off configuration for the small-scale model (fig. 5(b)). For the forward flap in the landing configuration (fig. 5(c)), the TF34 data follow the same trend as the data in the other parts of figure 5; but the small-

scale model data indicate a lower overall level and a much flatter spectrum, without a clearly definable frequency of peak response.

These data indicate that techniques using scaled geometry and the jet nozzle exit dynamic pressure, velocity, and diameter as parameters are sufficient to predict the loads on the flaps. However, some questions concerning the effects of temperature and noncircular nozzle exits still remain.

USB FLUCTUATING-LOADS STUDIES

Shown in figure 6 are photographs of the test configurations being used to study the USB fluctuating loads. Data on the fluctuating loads of each of these configurations have been or will be obtained. Starting at the upper left is an Aero Commander aircraft modified by the installation of over-the-wing JT15D engines (9 kN (2000 lb) thrust). Below that is a full-scale boilerplate model of the Aero Commander wing and flap, mounted upside down, also with a JT15D engine. In the lower left corner is a small-scale model of the boilerplate model using a cold air jet. Tests of the small-scale model are being conducted at the University of Virginia as part of a NASA study grant on powered-lift configurations. Results of these efforts are presented in reference 6.

At the upper right corner is an artist's sketch of the Boeing AMST YC-14. During the Air Force flight evaluation tests, the Boeing Company will obtain data on both the fluctuating loads and the interior noise levels for NASA. These tests are currently scheduled to start in the summer of 1976. Immediately below the YC-14 is a sketch of the YC-14 ground test rig. The Boeing Company, under contract to NASA, conducted tests on a full-scale mockup of the YC-14 using a combination of actual aircraft components and boilerplate components. Preliminary results from this test are reported in reference 7. Below the Boeing model is a photograph of the YC-14 scale model at Langley. Results on the USB static performance of the 1/4-scale model were presented in reference 8.

Wing Flap Loads

An example of the type of data obtained on the loads is shown in figure 7. The pressure spectra on the wing of the YC-14 scale model during engine run-up are shown in a "three-dimensional" format. A continuing spectral analysis, from 0 to 7 kHz in 20-Hz bandwidths, is performed while the engine thrust is increased from the value at idle speed (about 1100 N) to maximum thrust (7500 N). Each subsequent analysis is plotted just below the preceding one to form the picture shown in figure 7(b). This type of analysis presents a visual display of the continuous change in spectra with engine thrust. The fan tones and a compressor tone are clearly visible as peaks in the spectral curve, increasing in frequency as the thrust increases. Over the frequency range displayed, it may also be seen that with the exception of the engine tones, the spectra do not show any activity above 2 kHz. Below 2 kHz, the spectra vary as the thrust of the engine increases, and in figure 7(a) the section of the spectra shown by the dashed loop in figure 7(b) is expanded by analyzing the same data with a

4-Hz bandwidth over a frequency range of 0 to 500 Hz. Using this narrower band analysis shows that the frequency of the first peak in the response curve increases from about 100 Hz to 270 Hz for an increase in thrust from idle to maximum thrust. (See dashed lines in fig. 7(a).) Because the frequencies of peak response increase with thrust, a normalization such as Strouhal number would appear to be a reasonable approach to nondimensionalizing the frequency scale.

However, the problem may not be as straightforward as that for the EBF configurations. Shown in figure 8 are the fluctuating pressures along the projection of the engine center line for the USB boilerplate model of the Aero Commander. The OAFPL in decibels are shown at the right of the figure, with the maximum level of 156 dB occurring not in the impinged area, but somewhat downstream on the wing. Shown at the left of the figure are the power spectral densities of the fluctuating pressures associated with those overall levels. The 0 dB points on the vertical scale for each of the plots have been displaced so that the various spectra would not overlap. It may be observed that the spectra vary with the location on the wing or flap. At the impinged area (151 dB OAFPL), there are two peaks in the spectra: one at about 250 Hz. the other at 1700 Hz. Data from measurement locations downstream on the flap show a single peak emerging in the spectra and the frequency of this peak response decreasing. Near the flap trailing edge, the frequency of the peak response is 40 Hz. To normalize these data, it is apparent that the engine nozzle exhaust parameters would not be sufficient to collapse the levels and frequencies completely. Also, perhaps because of the nonsymmetrical shape of the nozzle, there appear to be at least two sources influencing the shape of the spectra at the impinged area. Continuing studies of the small-scale models should provide answers to some of these questions.

The studies on the Aero Commander model provided data on the structural response of a representative airframe structure. Although the structure of this model has been reinforced to support the engines and withstand the loads, it is clearly not a boilerplate model. Data reported in reference 9 showed rms levels as high as 38g occurring on panel sections in response to the flow over the upper surface of this structure. Shown in figure 9 are the responses of some of the main support structure in the area immersed in exhaust flow. The data are shown in terms of power spectral density plots of the pressure or acceleration. The two pressure spectra, one on the wing and one on the aft flap are similar to those reported in figure 8. The accelerations on the wing show several peak responses over the entire frequency range, although the maximum response is in the lower frequency range, where the pressure levels are the highest. An overall rms level of 4g was measured. The accelerometer on the flap was mounted on the flap track, a section of support structure connected all the way back to the wing. The acceleration spectrum also has several peaks with an overall rms level of 15g. Although the structure is responding very strongly to the excitation, in general the frequencies of peak responses in the wing do not match the frequencies of peak responses in the flap. This would indicate that the resonant responses of the structure are very localized and are not major overall vibration modes of the wing-flap system.

Fuselage Loads

The scale model of the YC-14 includes a section of fuselage. Shown in figure 10 are photographs of a tuft flow visualization pattern on this fuselage section. It should be noted that vortex generators to aid flow turning are installed. In figure 10(a), the engine is off and the tufts are hanging downward. In figure 10(b), the engine is running with an average jet exhaust velocity of 366 m/s. Along the bottom of the fuselage the tufts are almost horizontal; in the middle they are spinning around, as indicated by the blurred image; along the fairing they follow flow lines parallel to the flap contour; and on the top there is no indication of flow at all. In figure 11, the fluctuating pressure spectra at several locations on the fuselage are shown. The OAFPL's range from a high of 160 dB on the fairing section of the fuselage just off the trailing edge of the flap to a low of 144 dB on the top of the fuselage. This low measurement occurred in an area in which the tufts indicate no flow. The differences between the locations in the flow and the one location outside the flow may be better seen by looking at the spectra. Shown are the fluctuating levels, in decibels, analyzed by a constant-bandwidth filter having a nominal 20-Hz bandwidth. All the measurements made where the tufts indicate surface flow follow the same trend. Although the levels vary, all the spectra maximize at frequencies below 120 Hz. The measurements from the transducers located below the fuselage fairing have relatively flat responses below 120 Hz, whereas the measurements from the transducers on the upper sections of the fuselage peak at about that frequency. Above 120 Hz, the spectra all decrease at an approximate slope of 6 dB per octave. The spectrum measured outside the flow region had different characteristics. First, the peak in the response curve occurs at a somewhat higher frequency, centering at about 160 Hz; and the spectrum decreases at a much flatter slope, with levels above 1000 Hz actually higher than those measured by the two adjacent transducers. These data indicate that the higher levels and the lower frequencies are directly related to the exhaust flow; but even where there is no exhaust gas flow, acoustic levels are very high.

Although the conditions are not matched, the spectra in the exhaust gas flow areas shown here are very similar to the predicted spectra shown in figure 2, both in shape and level. This similarity indicates that the interior noise levels will be as high as predicted under some circumstances and that new techniques will have to be developed to help reduce these levels to current commercial aircraft levels.

CONCLUDING REMARKS

Measurements have been obtained from several EBF and USB test configurations ranging from small-scale models to large, full-scale models using actual jet engines. Data from these models are being evaluated at present, and initial results indicate that the anticipated high levels and low frequencies actually occur and will likely require special design considerations. The use of small-scale models to aid in predicting the loads and frequencies looks very promising, but additional development is still necessary and investigation into modeling is continuing.

Because initial predictions, partially supported by ground-test loads data, indicate high interior noise levels in powered-lift aircraft, Langley Research Center has extended its fluctuating-loads program into interior noise studies. Currently, measurements are being obtained on the AMST aircraft to aid in studies of sources and transmission paths of cabin interior noise in STOL aircraft.

The AMST flight test program, by obtaining measurements during actual operational conditions, should provide definitive data for evaluating the capabilities of scale-model prediction methods.

REFERENCES

1. Lansing, Donald L.; Mixson, John S.; Brown, Thomas J.; and Drischler, Joseph A.: Externally Blown Flap Dynamic Loads. STOL Technology, NASA SP-320, 1972, pp. 131-142.

2. Darton, C. Kearney: Interior Noise Consideration for Powered-Lift STOL Aircraft. NASA TM X-72675, 1975.

3. Hayden, Richard E.; Kadman, Yoram; and Chanaud, Robert C.: A Study of the Variable Impedance Surface Concept as a Means for Reducing Noise From Jet Interaction With Deployed Lift-Augmenting Flaps. NASA CR-112166, 1973.

4. Schoenster, James A.: Acoustic Loads on an Externally Blown Flap System Due to Impingement of a TF-34 Jet Engine Exhaust. NASA TM X-71950, 1974.

5. Mixson, John S.; Schoenster, James A.; and Willis, Conrad M.: Fluctuating Pressures on Aircraft Wing and Flap Surfaces Associated With Powered-Lift Systems. AIAA Paper 75-472, Mar. 1975.

6. Morton, J. B.; Haviland, J. K.; Catalano, G. D.; and Herling, W. W.: Investigations of Scaling Laws for Jet Impingement. Powered-Lift Aerodynamics and Acoustics, NASA SP-406, 1976. (Paper no. 28 of this compilation.)

7. Sussman, M. B.; Harkonen, D. L.; and Reed, J. B.: USB Environment Measurements Based on Full-Scale Static Engine Ground Tests. Powered-Lift Aerodynamics and Acoustics, NASA SP-406, 1976. (Paper no. 30 of this compilation.)

8. Hassell, James L., Jr.: Results of Static Tests of a 1/4-Scale Model of the Boeing YC-14 Powered-Lift System. Powered-Lift Aerodynamics and Acoustics, NASA SP-406, 1976. (Paper no. 3 of this compilation.)

9. Staff of Langley Research Center: Wind-Tunnel Investigation of the Aerodynamic Performance, Steady and Vibratory Loads, Surface Temperatures and Acoustic Characteristics of a Large-Scale Twin-Engine Upper-Surface Blown Jet-Flap Configuration. NASA TM X-72794, 1975.

TABLE I.-- OVERALL FLUCTUATING SURFACE PRESSURE LEVELS ON TF34 EBF MODEL

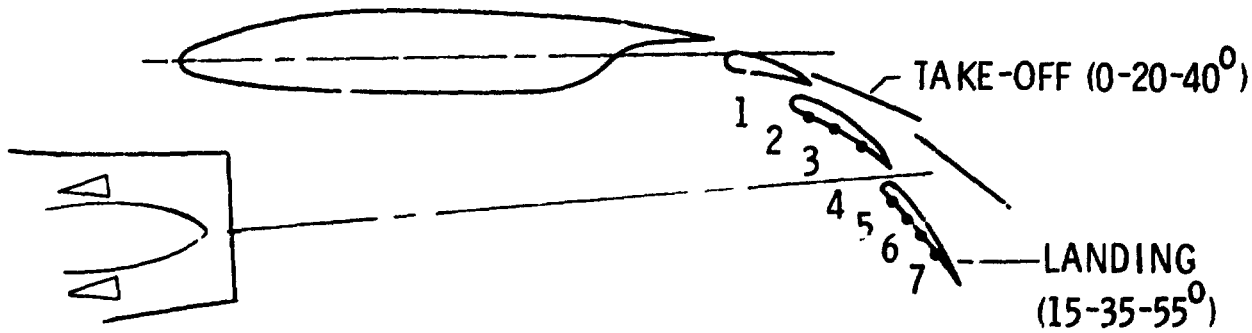

Transducer	OAFPL, dB (ref. 20 μPa), at Mach number of -									
	0.33	0.45	0.51	0.57	0.59	0.33	0.44	0.49	0.55	0.59
	Take-off flaps (0°-20°-40°)					Landing flaps (15°-35°-55°)				
1	149	155	156	158	159	150	156	158	160	(162)
2	151	157	159	160	161	148	154	156	159	160
3	152	158	160	162	(163)	148	153	155	157	159
4	149	154	156	159	160	(146)	152	153	156	157
5	145	150	152	155	156	147	152	154	156	156
6	(143)	148	150	152	153	148	154	155	156	157
7	144	149	151	---	154	148	153	155	157	157

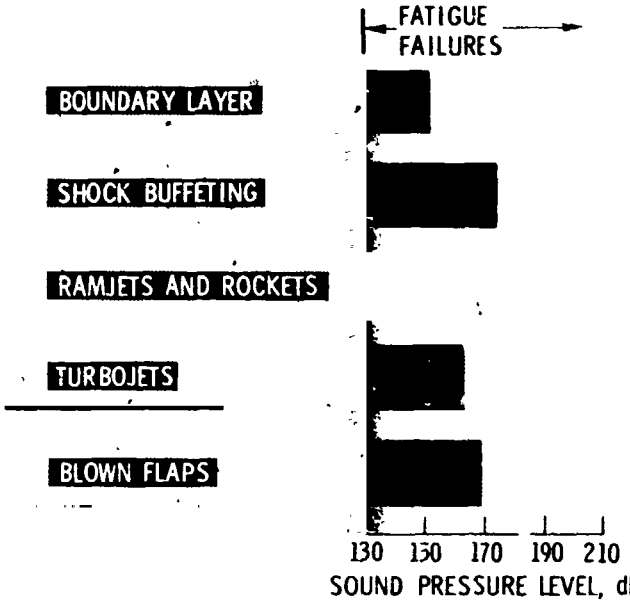

Figure 1.- Sound pressure levels of acoustic loading on aircraft structures (from ref. 1).

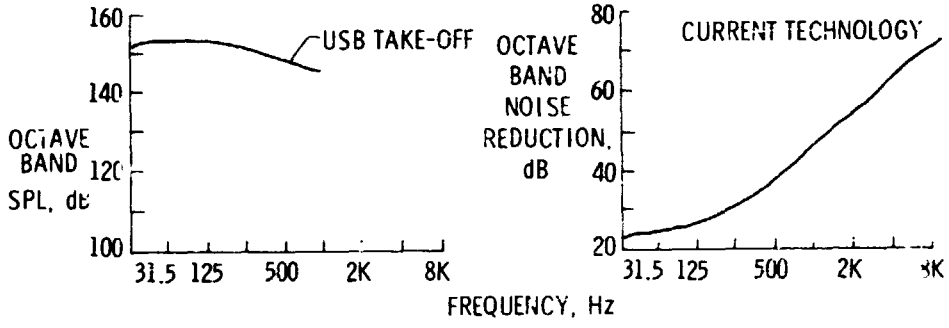

(a) External noise spectra.

(b) Sidewall noise reduction - current technology.

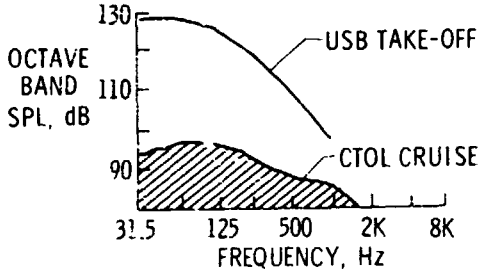

(c) Interior noise spectra.

Figure 2.- Estimated USB noise spectra (from ref. 2).

SCALING LAWS AND PREDICTION METHODS

SMALL-SCALE MODELS	LARGE-SCALE MODELS	FLIGHT TESTS
EBF MODEL (BBN)	TF34 EBF	AMST YC-15 (DOUGLAS) EBF
USB MODEL (U. VA.)	MODIFIED AERO COMMANDER-USB	AMST YC-14 (BOEING) USB
	BOILERPLATE MODEL-USB	
	YC-14 GROUND TEST-USB	
	YC-14 SCALE MODEL-USB	

Figure 3.- Program for development of prediction methods for fluctuating loads.

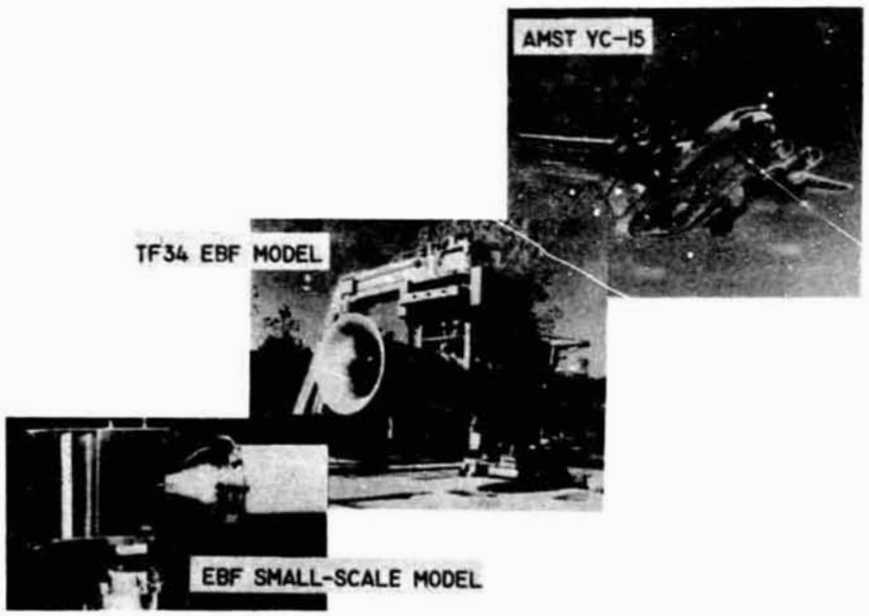

Figure 4.- Test configurations for EBF fluctuating-loads studies.

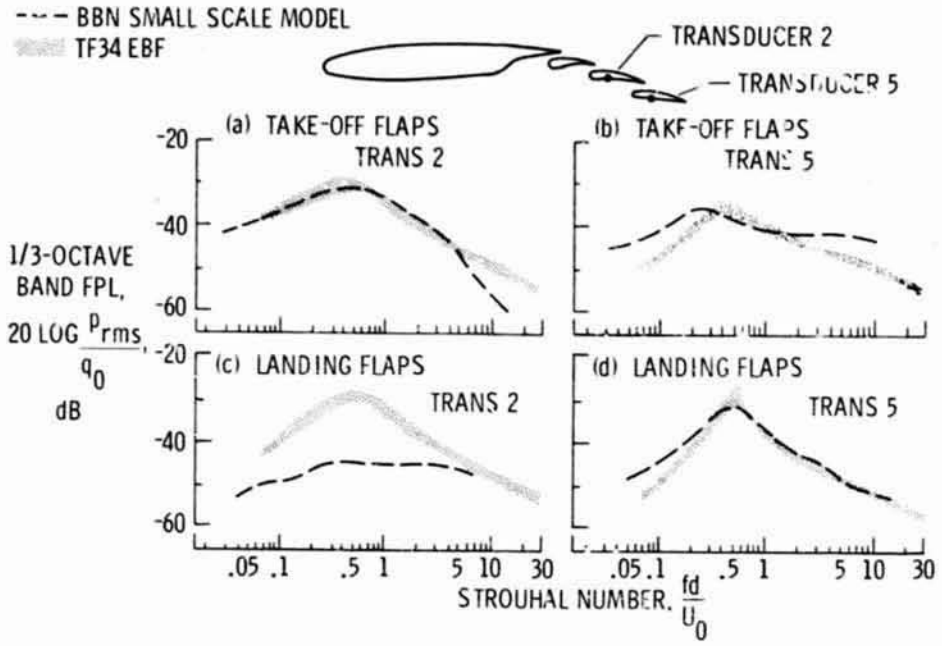

Figure 5.- Comparison of the fluctuating pressures on large- and small-scale EBF models.

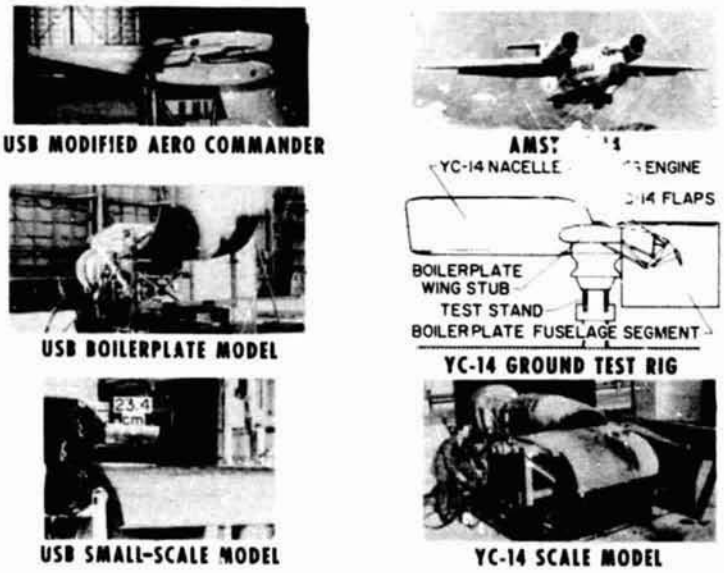

Figure 6.- Test configurations for USB fluctuating-loads studies.

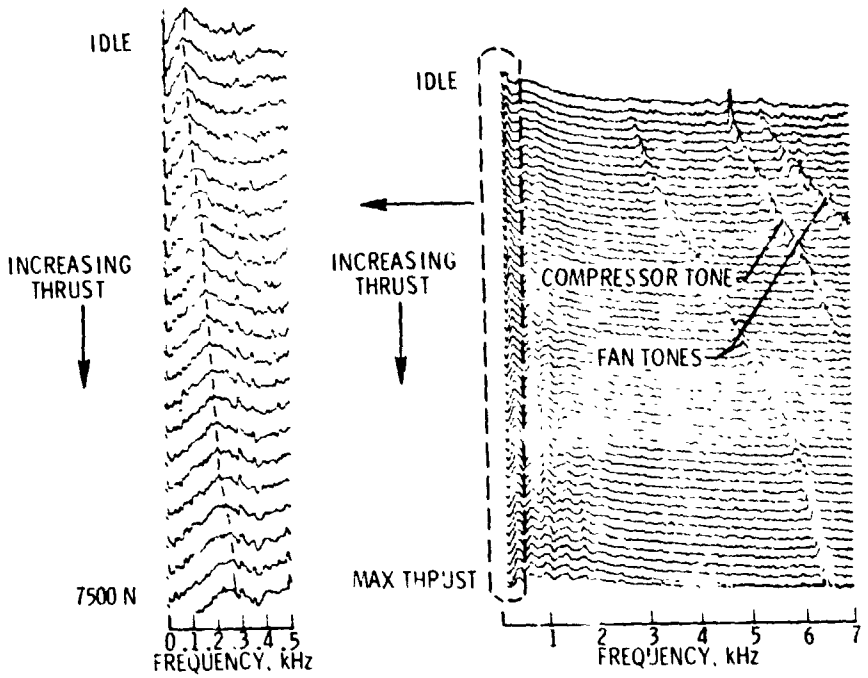

(a) 4-Hz bandwidth analysis.

(b) 20-Hz bandwidth analysis.

Figure 7.- Pressure spectra on wing of YC-14 scale model during engine run-up.

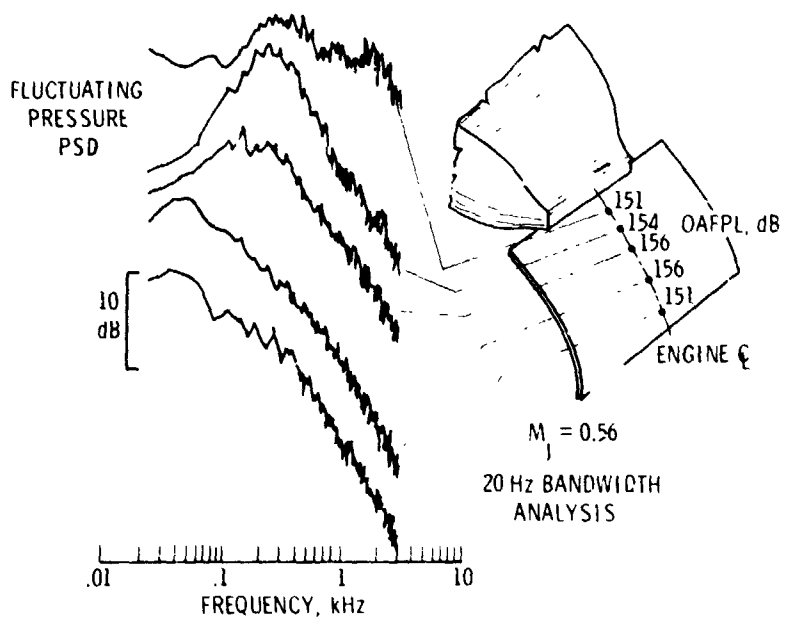

Figure 8.- Pressure spectra along engine center line of USB boilerplate model.

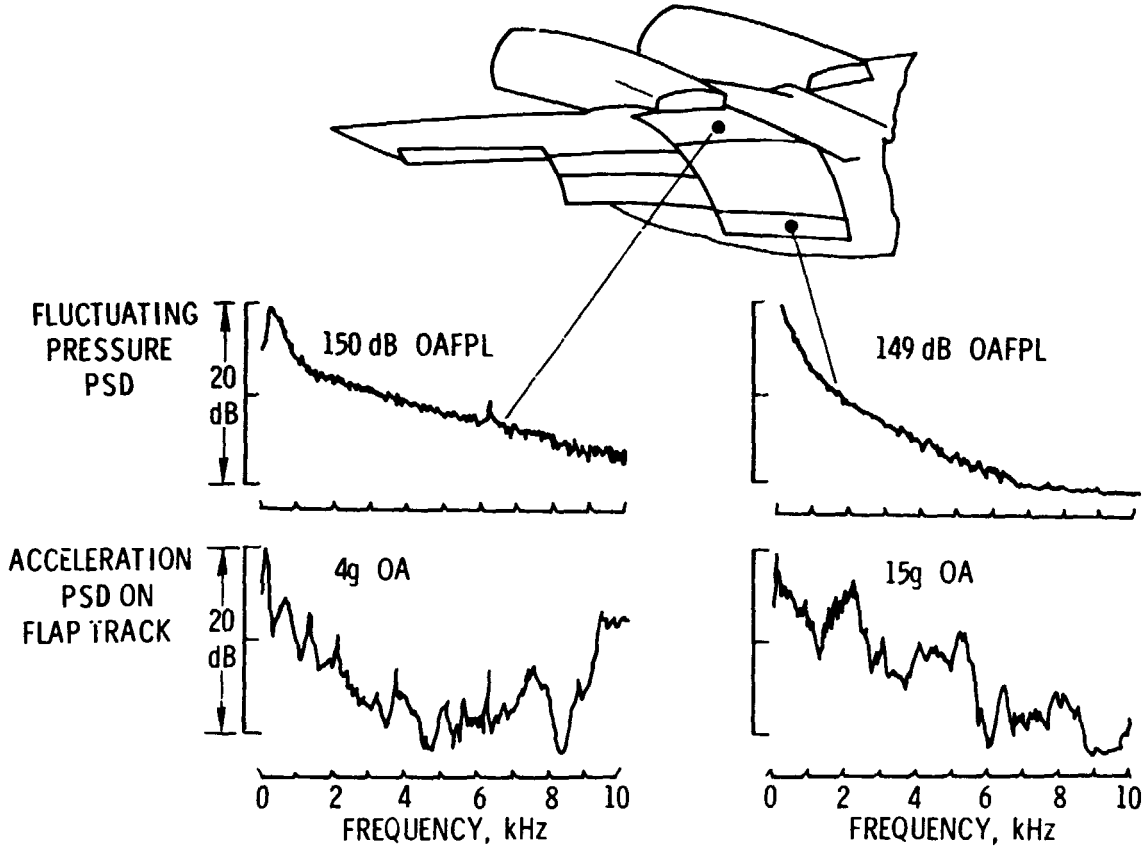

Figure 9.- Loads and response of wing and flap of USB modified Aero Commander.

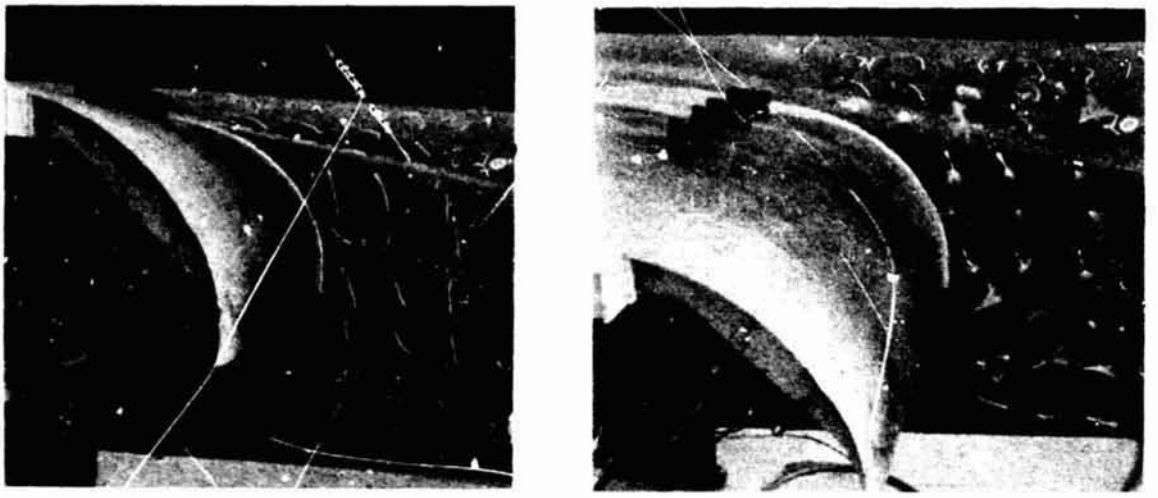

(a) Jet velocity: 0.

(b) Jet velocity: 366 m/s.

Figure 10.- Tuft flow patterns on fuselage surface of YC-14 scale model.

REPRODUCIBILITY OF THE
ORIGINAL PAGE IS POOR

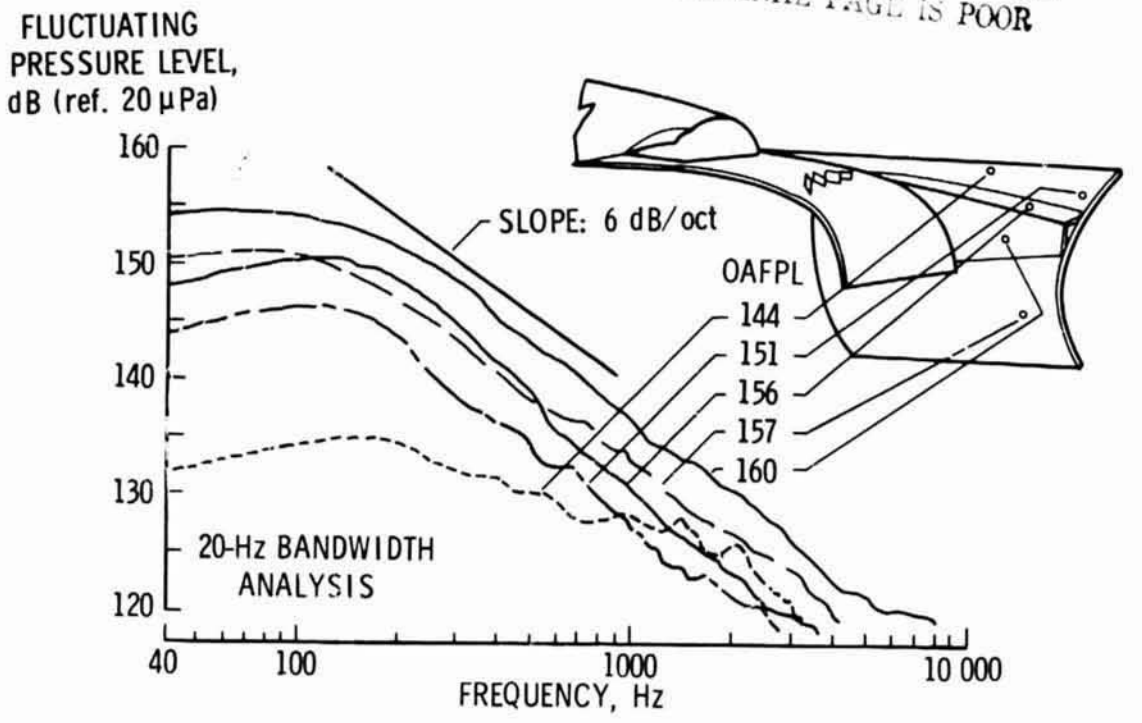

Figure 11.- Fluctuating pressures on fuselage sidewall of YC-14 scale model.